Chapter 2
Characterization and Dynamics of Polymer Microactuators

Beatriz Cristina López-Walle and Edgar Reyes-Melo

Abstract A magnetic hybrid material consisting of iron oxide nanoparticles (4 nm) embedded in a polymer matrix of Na-CMC was synthesized. The synthesis was done from a chemical treatment on a precursor hybrid material previously synthesized. The structure, morphology, and magnetic properties for this magnetic hybrid material were studied by X-ray diffraction, IR spectroscopy, transmission electron microscopy, and magnetometry. Additionally, the dynamic response was analyzed in order to probe the feasibility to use this magnetic hybrid material as a bending-type actuator. The experimental results show that the responses of the deflection have a linear trend over a reasonable range, suggesting that the magnetic hybrid material can be used as bending-type actuators in small mechanical systems and devices. First simulations have also been done considering the two components of the magnetic hybrid material: the oxide iron nanoparticles and Na-CMC. The displacement response takes in account the viscoelastic properties of the polymeric matrix and the magnetization of the nanoparticles.

2.1 Introduction

Recent advances in polymer science have allowed a better utilization of the properties of polymeric materials and their composite and/or hybrid materials [3, 10, 11, 17, 25, 27–30, 33, 39]. Polymers offer an attractive basis for microsystems [24]. Some of the characteristics of the polymer materials that benefit from both the field of microsystems and the electroactive polymer actuation technologies are: (1) elasticity, they can absorb impact energy and tolerate large degree of deformation;

B.C. López-Walle (✉) • E. Reyes-Melo
Programa Doctoral en Ingeniería de Materiales-FIME and Centro de Innovación, Investigación y Desarrollo en Ingeniería y Tecnología, Universidad Autónoma de Nuevo León, Av. Universidad s/n, Cuidad Universitaria, San Nicolás de los Garza, Nuevo León, México
e-mail: beatriz.lopezwl@uanl.edu.mx; mreyes@gama.fime.uanl.mx

M. Rakotondrabe (ed.), *Smart Materials-Based Actuators at the Micro/Nano-Scale: Characterization, Control, and Applications*, DOI 10.1007/978-1-4614-6684-0_2,
© Springer Science+Business Media New York 2013

(2) cost, they are relatively inexpensive compared to silicon; and (3) manufacturing, they can be formed into three-dimensional structures. In this chapter, a new hybrid material with potential applications as an electroactive microactuator is presented.

The synthesis of new hybrid materials has acquired great importance due to the development of experimental techniques allowing that two inherently incompatible components (e.g., organic polymers and inorganic oxides) can be combined by a pre-mix of both at the molecular level, before its conversion into a new hybrid material. This has allowed the design and synthesis of hybrid advanced materials with very specific physicochemical properties, including a multi-functional character, essential in modern organic electronics and microsystems. From the point of view of structure and morphology, a hybrid material is one phase or multi-phases dispersed into a matrix, which is typically a polymeric material. Additionally, the synthesis of hybrid materials with a polymeric matrix compatible to biological systems, as carboxymethyl cellulose or Na-CMC, represents an area that has paid a lot of attention of many research groups, due to the biological or surgical applications that this kind of materials could offer [30, 39]. The hybrid material described through the next sections is composed of a polymeric matrix of Na-CMC and inorganic nanoparticles of iron oxide (Fe_2O_3). Polymeric matrices are also suitable to encapsulate the metallic nanoparticles during their synthesis, avoiding the formation of agglomerates [3, 11, 26, 27, 29]. For these reasons, the development of hybrid magnetic materials using biocompatible polymeric matrices as Na-CMC is of great scientific and technological interest.

This work deals with a magnetic hybrid material based on Na-CMC and Fe_2O_3 nanoparticles. Section 2.2 describes the synthesis of this innovative material; Sect. 2.3 presents its structural, morphological, and magnetic characterization; and Sect. 2.4 shows the experimental results and finite element simulation (FES) of this material considering that it could work as a bending-type microactuator.

2.2 Synthesis of the Magnetic Hybrid Material

The synthesis of new hybrid materials by the scientific community has led to the improvement of the process of combining two or more materials with the purpose of obtaining multifunctional materials. In polymer technology, it is a common practice to strengthen conventional polymeric materials with inorganic fibers or fillers to improve their mechanical properties. This kind of materials have a great application today mainly for the construction of light vehicles and utensils for sports [8, 16]. In this sense, the development of new microactuators for the electronic industry, enabling it to extend their applications to biological systems, requires the synthesis of new hybrid materials with polymer matrix that respond to the application of a magnetic field [12, 18, 27, 29, 37], either, which can also carry electricity, without losing their viscoelastic properties and biocompatibility. To achieve these objectives, an important alternative is the development of nanostructured hybrid materials. Na-CMC due its low cost and its functional groups, it is a polymer matrix which

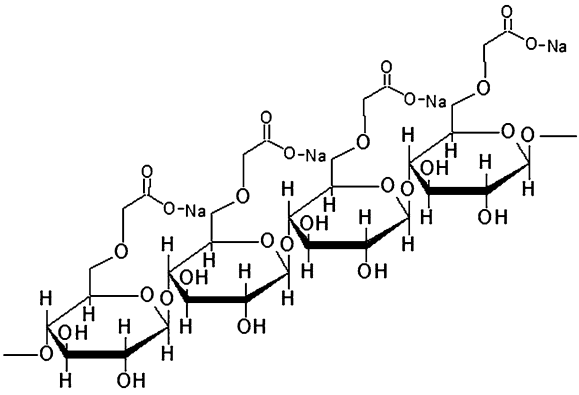

Fig. 2.1 Chemical structure of a chain segment of Na-CMC

can be used as a stabilizing agent of metallic nanoparticles. The aim of this section is the synthesis of magnetic nanoparticles that can be dispersed and stabilized in a polymeric matrix of Na-CMC, resulting in a hybrid magnetic material.

2.2.1 The Polymer Matrix or Na-CMC

Sodium carboxymethyl cellulose or Na-CMC is an ether derivative of cellulose with the carboxymethyl groups bounded to the hydroxyl groups of the β-anhydroglucose units (see Fig. 2.1) of cellulose macromolecules. The role of Na-CMC in the industry is related to its hydrophilic character and its high viscosity, allowing it to be used as base material to form thin films with good rheological properties. In addition Na-CMC also can be used as a thickener or even as adhesive in many industrial processes. In the process of Na-CMC synthesis, chemical groups of "sodium carboxymethyl" (CH_2COONa) are introduced in the repetitive units (β-anhydroglucose) of cellulose. These CH_2COONa groups give Na-CMC a certain degree of solubility in water; this property does not have cellulose macromolecules. Figure 2.1 shows a segment of Na-CMC chain, same hydroxyl groups have been replaced by sodium carboxymethyl groups into the repetitive unit: β-anhydroglucose. Because of its chemical structure, Na-CMC can form coordinate bonds with divalent ions without loss of its process ability [14, 15, 26, 28, 29, 36].

A very important aspect that defines the functional properties of Na-CMC is its degree of substitution or *DS*. The value of *DS* is a function of the average number of OH-groups replaced by CH_2COONa groups into the β-anhydroglucose units [26, 29]. Figure 2.1 shows that each β-anhydroglucose unit has 3 OH-groups available for a maximum of 3 *DS*. For example, in a sample of Na-CMC with a 1.5 *DS*, it means that on average 50% of the hydroxyl groups were replaced by CH_2COONa groups, and the 50% of remaining OH-groups remain free. The ability of the Na-CMC as a thickening agent for the control of flow of fluids (rheology control) depends largely on its *DS* value. At the same time the magnitude of *DS*

depends on reaction kinetics for the synthesis of Na-CMC. For samples with low values of *DS*, for example $DS = 0.2$, most of the reaction was carried out in amorphous cellulose regions or on the surface, and consequently Na-CMC sample is relatively insoluble in water, but it absorbs significantly more liquid than the starting (cellulose) material. For values of $DS = 0.5$, Na-CMC shows partial solubility, due to little replaced regions that appear very swollen and opaque, as an opaque gel. Samples with a $DS = 0.7$ or greater are the result of sufficient replacement of OH-groups producing a higher solubility of Na-CMC in water and minimize the physical interactions among chains that produce agglomerates, these interactions can be interrupted by the inherent stress in the fluid and produce thixotropic rheology. The chemical reactions necessary for the synthesis of Na-CMC, which reach a value of $DS = 1$, produce polymeric chains that have a very low concentration of OH-groups; these OH-groups have not been replaced by carboxymethyl groups. Consequently this specimen has a little tendency to the formation of agglomerates. These last aspects lead to a rheology behavior of Na-CMC which is known as pseudoplastic (or non-Newtonian rheology). In pseudoplastic behavior viscosity decreases as shear rate increases. It is important to remark here that when OH-groups into chains of Na-CMC are uniformly replaced by CH_2COONa groups, these groups interact with water molecules producing a uniform flow of Na-CMC solution. On the other hand, when OH-groups are replaced by CH_2COONa groups at a random way, the less substituted regions or hydrophobic chains, they tend to swell, since these regions tend to be associated through hydrogen bonds and form three-dimensional networks that give rise to a structure with thixotropic fluid characteristics. Na-CMC compatibility is another important property that is also affected by *DS*-magnitude; this is because the less soluble regions of Na-CMC tend to precipitate easily. Na-CMC samples with high values of *DS* which correspond to Na-CMC uniformly replaced are more stable to acid pH, because of that acid hydrolysis takes place in the union ether between two β-anhydroglucoses units. An important technological information of commercial Na-CMC is as follows, it is solid white, odorless, tasteless, and without toxicity. Viscosity in aqueous solutions to 2% ranges between 10 and 50,000 mPa s [26].

2.2.2 In Situ Synthesis of the Magnetic Hybrid Material

Today, a wide variety of methodologies that allow a combination at the molecular level of different materials have been developed. Many of these methodologies are based on some mechanism of precipitation, controlling the size of particle produced in this way [3, 26, 28, 29]. These methodologies for the synthesis of hybrid materials are classified as in situ and ex situ methodologies. For methodologies classified as in situ growth of nanoparticles is given into the polymer matrix, instead on methodologies ex situ nanoparticles are synthesized independently and then they are dispersed into polymer matrix. In this work, we used an in situ methodology to obtain a magnetic hybrid material (Fe_2O_3/Na-CMC).

For in situ methodologies, it is essential that, at a first stage must be mixed inorganic precursors with the polymer matrix, and then inorganic precursors into polymer matrix are transformed to a new phase. The pre-mix can be carried out in several ways:

- Absorption of metal ions in ion-exchange resin or polymeric gels
- Dissolution of precursors in a polymer solution
- Deposition of precursors in a porous polymer, chemical, electrochemical methods or steam

A prerequisite for the development of the in situ methodology is that the polymer matrix must have functional groups, which should be establishing chemical or physical interactions with the metallic ions of precursor salts, favoring a homogeneous dispersion of the precursor salt into the matrix. Once the metallic ions interact with the polymer matrix, a chemical or physical treatment is carried out with the purpose of obtaining the desired structure of the dispersed phase. In a previous work, it has been reported the synthesis of a material hybrid in which were dispersed in a homogeneous way nanoparticles of Fe_2O_3 into a polymeric matrix of chitosan [27].

For the synthesis of Fe_2O_3/Na-CMC hybrid material, the process was carried out in two stages. In the first stage, the main objective is that the precursor salt and Na-CMC should be combined in a way such that the precursor salt ions are dispersed evenly in the Na-CMC, to obtain a precursor hybrid material. In the second stage, the precursor hybrid material is subjected to a certain chemical treatment for obtaining Fe_2O_3/Na-CMC.

Figure 2.2 is a schema of the first stage; Na-CMC and $FeCl_2$–$4H_2O$ were dissolved in distilled water obtaining two solutions Na-CMC/H_2O and $FeCl_2$/H_2O. Both solutions were subjected to an agitation process for 5 h, and then mix both solutions; the product obtained is subjected to another agitation process during 4 h. After that, this last solution is poured in a Petri dish and is subjected to a process of drying by natural convection in a hot plate at an average temperature of 40 °C for 24 h. The resulting product is the precursor hybrid material. This material is stored in a desiccator where samples are taken for analysis and also to be subjected to chemical treatment that constitutes the second stage.

In the second stage, the precursor hybrid material was subjected to a chemical treatment with an aqueous solution of NaOH 6.7 M at 40 °C. Consequently the precursor hybrid material undergoes a change of color, dark coffee to black. After that, the "black" material is immersed in the alkaline solution and then 30 mL of hydrogen peroxide (H_2O_2) was added, this produced a new change of color, black to reddish brown. After 15 min the "reddish brown" material was removed from the alkaline solution and it was subjected to a process of washing with distilled water and ethyl alcohol, with the aim of eliminating waste substances. This new material is the final product that presumably is a hybrid magnetic material composed of Fe_2O_3 nanoparticles dispersed in a polymer matrix of Na-CMC.

The magnetic hybrid material obtained has been characterized structurally, morphologically, and magnetically. The techniques applied and the results obtained are described in the next section.

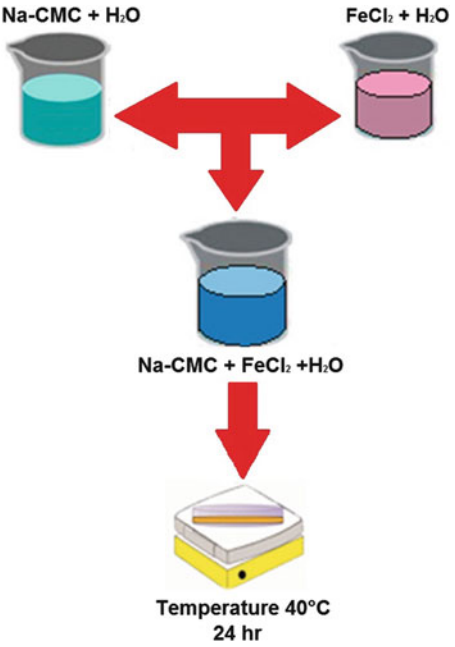

Fig. 2.2 First step of the synthesis of the magnetic hybrid material: the precursor hybrid material

2.3 Characterization of the Magnetic Hybrid Material

In this section, the experimental results obtained from the structural, morphological, and magnetic characterizations are presented and discussed. In the first part, we deal with the structure and morphology for both the precursor hybrid material and the magnetic hybrid material. In the second part, the magnetic properties of the last one are analyzed.

2.3.1 Morphology and Structure of the Precursor Hybrid Material and the Magnetic Hybrid Material

For the synthesis of the precursor hybrid material two aqueous solutions were mixed, one of $FeCl_2$ and another of Na-CMC, this with the purpose of obtaining an aqueous solution containing $FeCl_2$ and Na-CMC. After that, it has removed the solvent by natural convection; it allowed us to obtain a thin film in which presumably the Fe^{2+} ions are bound to carboxymethyl groups of the Na-CMC. Figure 2.3 shows three images, the first one (Fig. 2.3a) is a thin film of Na-CMC, the second one (Fig. 2.3b) corresponds to a film of the precursor hybrid material, and Fig. 2.3c is a powder of the magnetic hybrid material obtained.

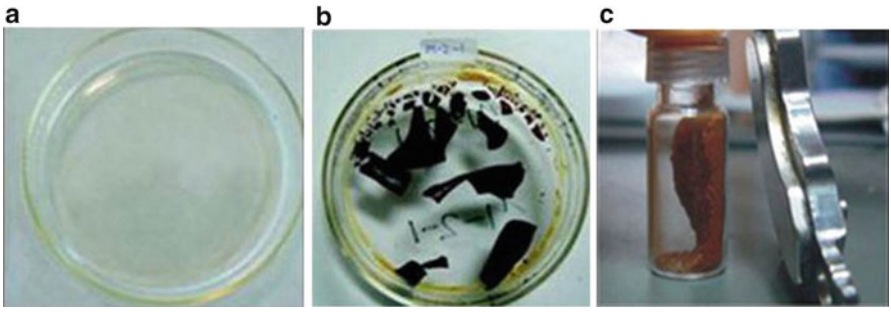

Fig. 2.3 The magnetic hybrid material at different steps: (**a**) Na-CMC sample, (**b**) the precursor hybrid material, and (**c**) powder of the magnetic hybrid material

In order to verify that the Fe^{2+} ions have some kind of chemical interaction with carboxymethyl groups of Na-CMC, the precursor hybrid material (Fig. 2.3b) was analyzed by X-ray spectroscopy and IR-spectroscopy. On the one hand, the X-ray diffraction technique was used mainly to corroborate the complete dissolution of precursor salt into the polymer matrix of Na-CMC. The device used was a SIEMENS D5000 diffractometer with a radiation source of CuK. On the other hand, by IR-spectroscopy, the different vibration modes of the chemical groups for both the precursor hybrid material and Na-CMC samples were analyzed. Using these results, it was possible to study the interactions between functional groups of the Na-CMC and the ions of precursor salt. The device used to obtain these experimental measurements was a Nicolet FTIR spectrometer.

Figure 2.4 shows the patterns of X-ray diffraction which were obtained for the samples of Na-CMC (Fig. 2.4a), for the precursor hybrid material in question (Fig. 2.4b), and for salt precursor $FeCl_2{\cdot}4H_2O$ (Fig. 2.4c). The diffractogram obtained for Na-CMC sample (Fig. 2.4a) is a typical curve corresponding to materials with amorphous structure. While the diffraction pattern that corresponds to the precursor hybrid material is displayed in Fig. 2.4b. It is clear that the diffraction peaks in Fig. 2.4b do not correspond to the precursor salt, $FeCl_2{\cdot}4H_2O$, see Fig. 2.4c, these diffraction peaks correspond to NaCl crystals embedded into Na-CMC matrix. These results suggest that the precursor salt ($FeCl_2{\cdot}4H_2O$) was completely dissolved into the polymer matrix, probably forming chemical bonds between Fe^{2+} ions and carboxymethyl groups of the Na-CMC. On the other hand, the presence of crystals of NaCl into the precursor material is a consequence that in the first stage of the synthesis process, there are conditions to carry out a process of crystallization, due to the ionic interactions that occur between the Cl^- of the precursor salt and the Na^+ from the Na-CMC [26, 29]. In order to corroborate the chemical interaction of ions of Fe^{2+} with the Na-CMC, the different modes of vibration which have functional groups both the precursor hybrid material and Na-CMC samples were determined by IR-spectroscopy. The comparison of the spectra obtained for these samples (see Fig. 2.5) go allowed clarifying the way in which Fe^{2+} ions interact with the polymer matrix for the formation of the precursor hybrid material.

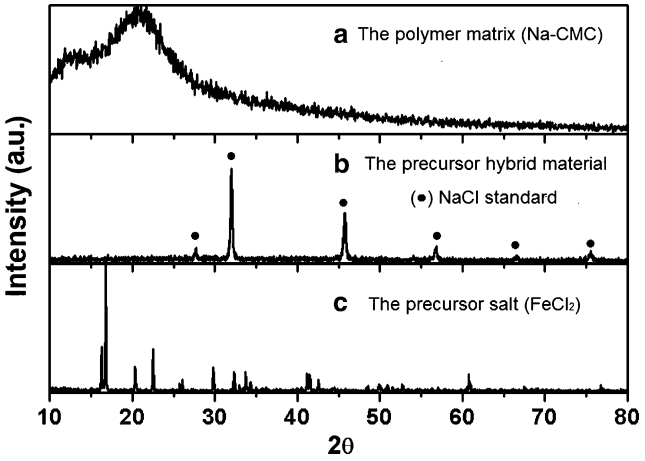

Fig. 2.4 X-ray diffraction patterns for samples: (**a**) Na-CMC, (**b**) the precursor hybrid material, and (**c**) precursor salt ($FeCl_2 \cdot 4H_2O$)

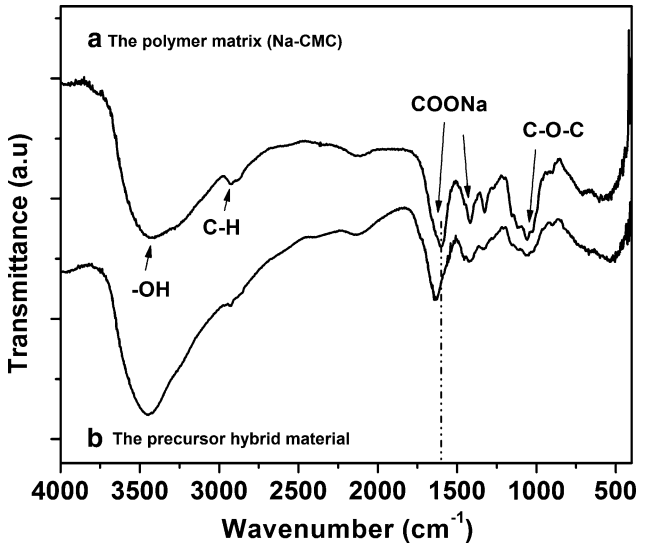

Fig. 2.5 Infrared spectra for: (**a**) NA-CMC and (**b**) the precursor hybrid material

Figure 2.5a corresponds to the infrared (IR) spectrum obtained for Na-CMC sample. The characteristic vibration mode associated with chemical groups –OH is observed at 3,500 cm^{-1}. Another vibration mode is stretching of C–H, and its corresponding band is observed at 2,925 cm^{-1}. At 1,417, 1,600, and 1,058 cm^{-1} are identified another bands related to stretching of the asymmetric ether group of the carboxymethyl groups. On the other hand, Fig. 2.5b corresponds to infrared

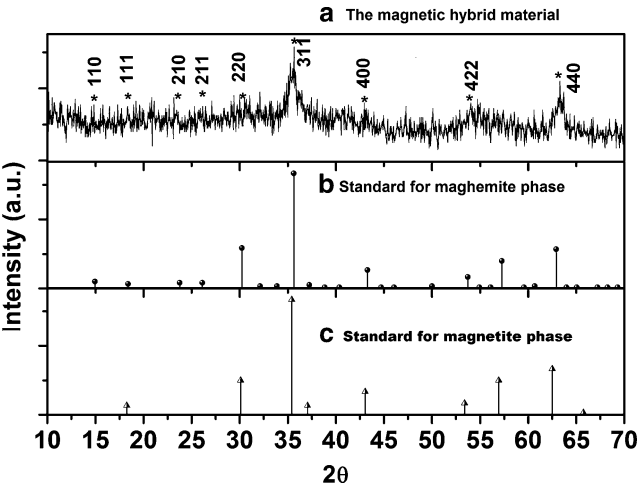

Fig. 2.6 Diffraction patterns for: (**a**) the magnetic hybrid material, (**b**) standard maghemite phase, and (**c**) standard magnetite phase

spectrum of the precursor hybrid material; in this figure the band associated with the carboxymethyl groups has a shift towards high values of the wavenumber, about 1,633 cm^{-1}. The shift of this band is related to chemical interactions that occur between Fe^{2+} ions and carboxymethyl groups of Na-CMC. The results obtained by X-ray diffraction and IR-spectroscopy allow us to ensure that Fe^{2+} ions are distributed evenly in the polymer matrix of the precursor hybrid material. This condition is necessary and indispensable for the precursor hybrid material to be used as raw material base for the synthesis of Fe_2O_3 nanoparticles homogeneously dispersed into Na-CMC.

The hybrid magnetic material samples were also analyzed by X-ray diffraction with the aim of determining the crystal structure and the size of nanoparticles dispersed into polymer matrix. The Scherrer equation [26, 29] was used for the calculus of particle size [26]. Figure 2.6a shows the diffraction pattern obtained for the magnetic hybrid material. The diffraction peaks which are marked with an asterisk (*) 18.35°, 30.25°, 33.65°, 42.25°, 53.7°, and 62.95° correspond to crystallographic planes (1 1 1), (2 2 0), (3 1 1), (4 0 0), (4 2 2), and (4 4 0), respectively, and they are consistent with the bars shown in Fig. 2.6b coming from a standard diffraction phase of maghemite [1 0 0], and also with standard diffraction phase (Fig. 2.6c) of magnetite [1 0 1]. In addition, it also displayed diffraction peaks associated with the crystallographic planes (2 1 0), (2 1 1), and (1 1 0) belonging to the phase of maghemite [1 0 0]. These results are important since they corroborate us the existence of a phase Fe_2O_3 into the polymer matrix of Na-CMC [26, 29].

From experimental results of Fig. 2.6a, inter-planar distances (d) were calculated using Bragg law. These calculated values of d are consistent with those reported in the literature for the crystal structure of the [1 0 0] maghemite. Table 2.1 shows

Table 2.1 Computed inter-planar distances $d = d(d_{exp})$ from experimental results

$2\theta_{exp}$	d	$d(\gamma Fe_2O_3)$	$d(Fe_3O_4)$
14.95	0.5921	0.5918	
18.35	0.4800	0.4822	0.4852
23.75	0.3740	0.3740	
26.10	0.3411	0.3411	
30.25	0.2952	0.2953	0.2967
35.65	0.2516	0.2517	0.2532
43.25	0.2090	0.2088	0.2099
53.70	0.1705	0.1704	0.1714
62.95	0.1475	0.1475	0.1484

d-computed values and the reported values in ICDD database for maghemite $d(\gamma Fe_2O_3)$ and magnetite $d(Fe_3O_4)$ phases. The computed d values are very close to the ICDD values for maghemite crystalline structure [26, 29].

On the other hand, from the experimental data of Fig. 2.6a, it is also possible to compute the crystal size $\langle L \rangle$ by Scherrer equation:

$$\langle L \rangle = \frac{0.89\lambda}{\beta \cos\theta} \tag{2.1}$$

where λ is the wavelength of the incident X-rays, θ is the half of the diffraction angle 2θ in degrees, and β is the full width at half maximum of the diffraction peak. The computed value $\langle L \rangle$ obtained was 5.6 nm. These results suggest that iron oxide nanoparticles are embedded into the polymer matrix.

To obtain additional information about the chemical structure of the magnetic hybrid material, an IR-spectroscopy analysis was performed. Results are displayed in Fig. 2.7. The IR-spectrum obtained in Fig. 2.7b shows the characteristic bands of Na-CMC at 3,500, 2,925, and 1,058 cm^{-1} already mentioned. In this case, unlike the IR-spectrum of the precursor hybrid material (Fig. 2.5b), the bands associated with the carboxymethyl groups remain at 1,600 and 1,417 cm^{-1} for the magnetic hybrid material.

This result can be interpreted as a weak-chemical interaction between iron oxide nanoparticles and the carboxymethyl groups of the Na-CMC. In addition, the band at 1,600 cm^{-1} also suggests that during the iron oxide precipitation, the sodium-carboxymethyl groups were again formed through the reaction of carboxymethyl groups with Na^+ of NaOH added to obtain alkaline conditions (see Fig. 2.8). It is important to remark here the presence of two peaks in the IR-spectrum for magnetic hybrid material (Fig. 2.7b), they are located at 570 and 437 cm^{-1} wavenumber. In [26, 29], these bands were associated with the Fe–O bending vibrations of the maghemite iron oxide phase.

The size and morphology of Fe_2O_3 nanoparticles into magnetic hybrid material were studied by Scanning Transmission Electron Microscope (STEM) and High-Resolution Transmission Electron Microscope (HRTEM) techniques. A scanning electron microscope JEOL 2010 transmission with acceleration 200 kV voltage was used for this purpose. For this analysis, samples were prepared in the form of powder as the specimen shown in Fig. 2.3c, and they were subsequently dispersed

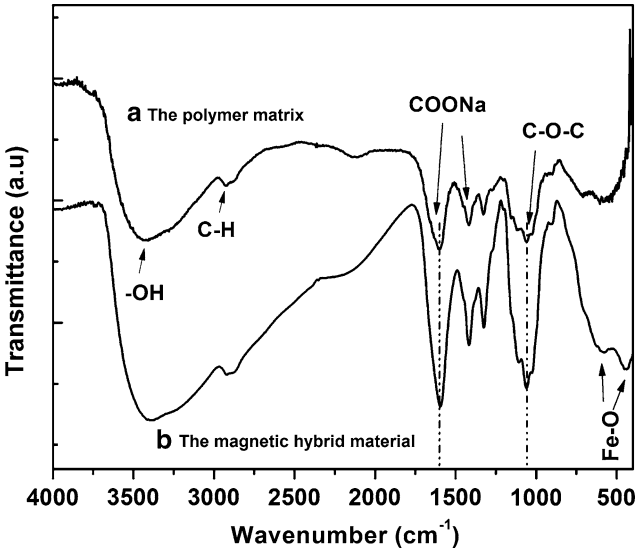

Fig. 2.7 IR spectra for: (**a**) Na-CMC and (**b**) the magnetic hybrid material

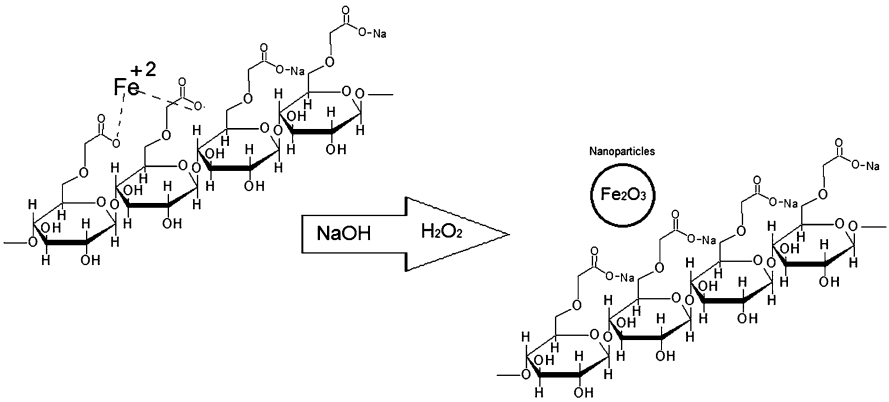

Fig. 2.8 Schematic representation of the synthesis process of magnetic hybrid material from a precursor hybrid material

in acetone, using for this purpose a sonificator (ultrasound). After that, it is taken an aliquot and settles on a grid of copper-coated with a film of carbon.

The STEM images (Fig. 2.9) show a higher number of iron oxide nanoparticles with sphere-like morphology. The average particle size of the iron oxide was measured using image analysis, and the frequency histogram shows a size of 4 nm (inset Fig. 2.9), very similar to the previously computed value $\langle L \rangle$ obtained using the Scherrer equation.

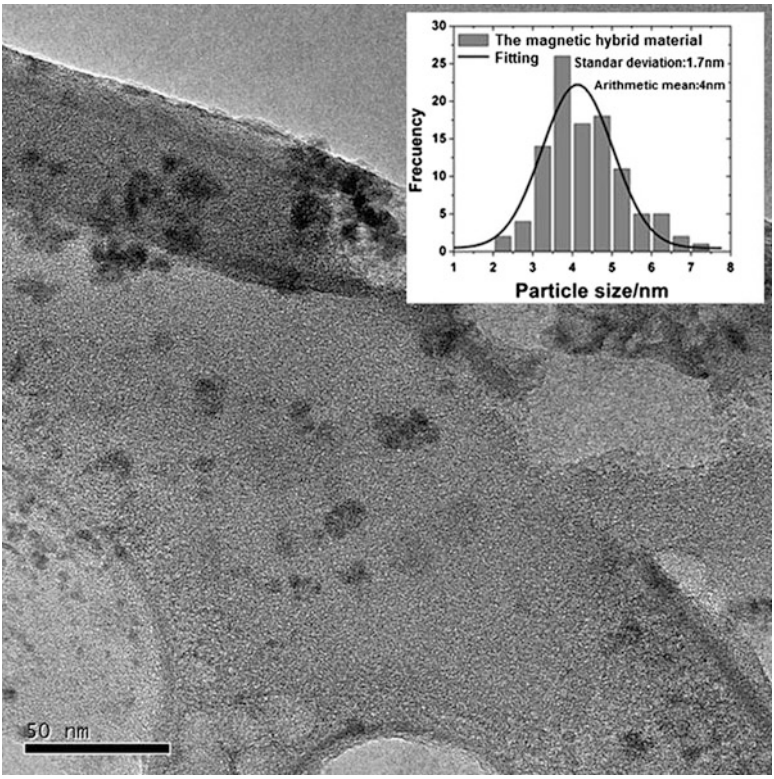

Fig. 2.9 STEM image of the magnetic hybrid material and frequency histogram

HRTEM image of Fe_2O_3 nanoparticles is shown in Fig. 2.10. The well-defined lattice fringes correspond to crystallographic planes of Fe_2O_3 nanoparticles and they are identified in this HRTEM image. In addition, inter-planar distances: 0.477, 0.332, 0.297, and 0.249 nm were also computed from this figure. These computed values correspond to inter-planar distances of (1 1 1), (2 1 1), (2 2 0), and (3 1 1) planes. These crystallographic planes are of maghemite crystalline structure, which is consistent with the X-ray diffraction analysis. These inter-planar distances are very close to the computed values, shown in Table 2.1.

The study of the structure and morphology of the magnetic hybrid material indicates that iron oxide nanoparticles are evenly dispersed in the polymer matrix. The following section presents the results obtained from the analysis of the magnetic behavior of the magnetic hybrid material.

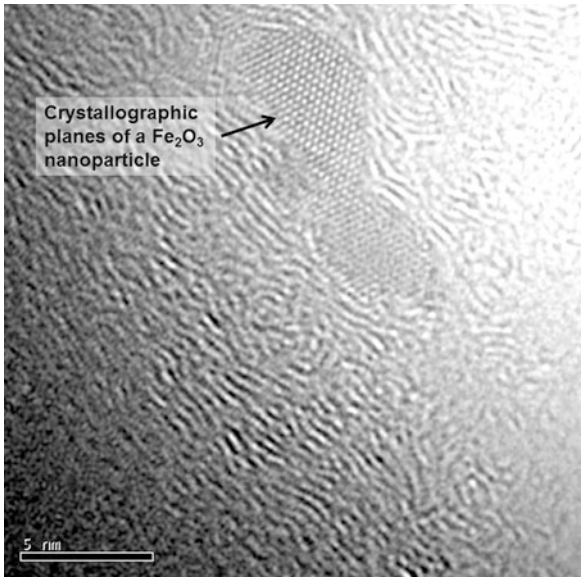

Fig. 2.10 HRTEM images of Fe_2O_3 nanocrystals into the magnetic hybrid material

2.3.2 *Magnetic Properties of Magnetic Hybrid Materials*

The magnetic hybrid material (Fe_2O_3/Na-CMC) was synthesized by subjecting the precursor hybrid material to a chemical treatment in an alkaline solution and hydrogen peroxide. At this stage it changed its color to black when the precursor hybrid material is in contact with the alkaline solution, then to reddish brown by gradually adding the peroxide. This color change is considered a macroscopic evidence of the formation of nanoparticles of iron oxide (in situ) in the polymer matrix of the CMC, obtaining with this a magnetic hybrid material, Fe_2O_3/Na-CMC. For the study of magnetic properties, the samples of the magnetic hybrid material were powdered as the specimen shown in Fig. 2.3c.

The study of the magnetic properties of the synthesized hybrid magnetic material was carried out through a Quantum Design MPMS magnetometer of the SQUID VSM type by magnetization measurements. Figure 2.11 shows the magnetization curve at room temperature (300 K). The saturation magnetization value (Ms) is 13.9 emu/g whereas both, remnant magnetization and coercivity (Hc) are undetectable. These last results are characteristics of a magnetic hybrid material with superparamagnetic behavior.

Conversely, Fig. 2.12 presents the magnetization curve at temperature 2 K. Under these conditions both coercivity field and remanent magnetization values are different to zero. It can be seen that the corresponding values for the different magnetic parameters are 19.9 emu/g for saturation magnetization, 357 Oe for coercive field (Hc), and 6.14 emu/g for remanence value (Mr) (inset Fig. 2.12); a ferromagnetic behavior appears when the magnetic analysis is performed below the blocking temperature (TB).

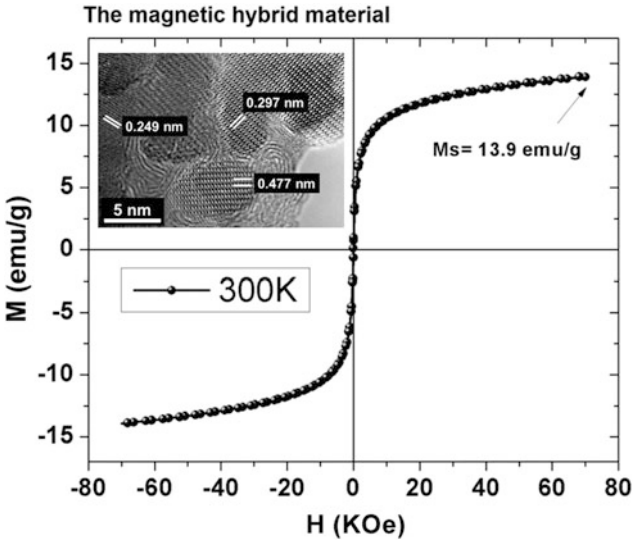

Fig. 2.11 Magnetization curve for the magnetic hybrid material at room temperature

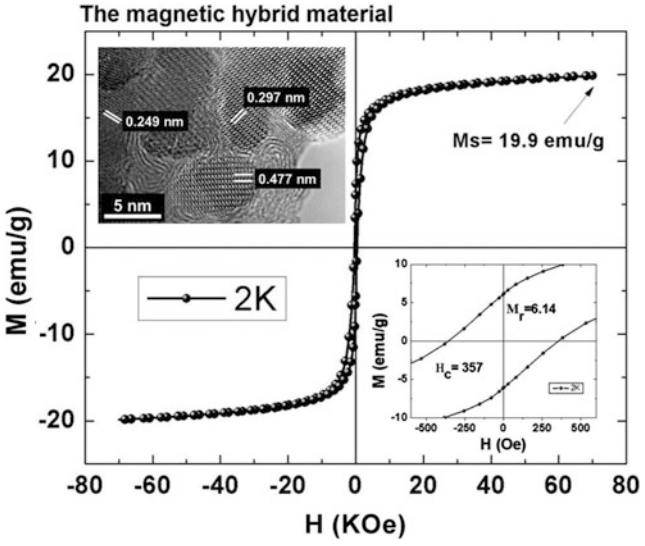

Fig. 2.12 Magnetization curve for the magnetic hybrid material at 2 K

To estimate the *TB* for the magnetic hybrid material, cooling at zero magnetic field (ZFC) and field cooling (FC) analyses was performed at a magnetic field of 100 Oe (Fig. 2.13). When the magnetic hybrid material is cooled at ZFC, Fig. 2.13 shows that the total magnetization is small, but not zero (20% of the maximum),

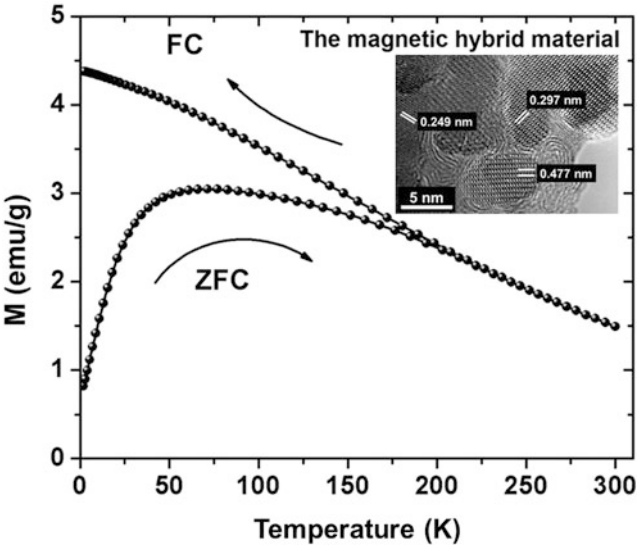

Fig. 2.13 ZFC and FC magnetization curves at 100 Oe

as the magnetic particles are not fully random. When temperature increases, the nanoparticle magnetic moment is oriented with the external field increasing the total magnetization until it reaches a maximum at 71 K which is the value of the blocking temperature (TB). At this temperature, the thermal energy becomes comparable to the energy gained by aligning the nanoparticle magnetic vector in the weak field. At this point, the transition from ferromagnetic to superparamagnetic behavior is observed. When all nanoparticles are at the superparamagnetic relaxation state, above TB, their magnetization follows Curie's law decreasing with increasing temperature. In the case of field cooling (FC), magnetization monotonically increases as the temperature decreases because the nanoparticles are cooled from room temperature under a magnetic field and the magnetization direction of all the nanoparticles is frozen in the field direction. The magnetization shows the maximum at 2 K in the FC process (Fig. 2.13).

In conclusion, the analysis of the magnetic properties of the magnetic hybrid material shows a superparamagnetic behavior at room temperature changing to ferromagnetic below 71 K, the blocking temperature.

The next section presents the experimental and FES response of the magnetic hybrid material for working as a bending-type actuator.

2.4 Actuation Properties of the Magnetic Hybrid Material

Electroactive materials with low driving voltage and large displacement are of critical importance for advancing the technology of microactuation. The major drawbacks of magnetic actuation are the by-effects arising from the relatively high currents involved in conventional magnetic actuation: the Joule losses in conductors imply overheating which may call for cooling techniques but also energy wastage [7]. The innovative material described above mixes the magnetic properties of the Fe_2O_3 and the insulating characteristics of the polymeric Na-CMC. Hence, it presents a good response face to an external magnetic field, but it does not heat because of the Joule effect.

Even if electromagnetic systems typically are rather complex, not only does magnetism already dominate the macroworld, but it also scales down very well to the microworld. Electromagnetic interactions that deserve a larger interest from the microsystems community, magnetic fields, and gradients can be effective over long distances relatively to the size of the microsystems. Additionally, magnetic microsystems offer large forces, large strokes, remote or distance control, bi-stability, robustness, high energy conversion efficiency, levitation, etc., all with great potential for new devices in many domains of applications.

The global market for magnetic sensors has been growing in terms of technology and applications. Position sensors, speed sensors, and record heads in hard disk drives in computers are the most commonly used magnetic sensor types currently in vogue. One of the rapidly expanding application areas includes e-compassing used in passenger cars, GPS-enabled handheld devices, cell phones and dead reckoning (DR) in personal vehicle, aircraft and marine navigation [32]. Contactless magnetic interaction allows remote actuation making magnetic actuators very well suited to harsh environment or for medical applications, through the skin. Laboratory-developed prototypes include RF microswitches for mobile phones, read/write heads and microposition systems, optical microcross-connect for fiber optic networks, microscanners, micromotors for less-invasive surgery or microrobotics, micropumps or microvalves for lab-on-chip and microfluidic devices, electrical microgenerators for autonomous power supplies, micromirrors for adaptive optics, microscanners for retinal scanning displays, magnetic suspensions for hard disk drives, etc. [7, 20, 22, 35, 38].

For these innovative applications, the insertion of smart functions was not previously possible with macroscopic devices. Performing research in the field of magnetic microactuators becomes thus a necessity. This section deals with the actuation properties of the magnetic hybrid material (Na-CMC/Fe_2O_3). As it has been explained, the hybrid material reacts to external magnetic fields. The resulting motion and force could be used as a magnetic field-controlled actuator. The focus of the macroscopic study of the magnetic behavior of the magnetic hybrid material is to investigate its dynamic response, specifically the displacement curves as a function of the applied magnetic field. This study has been performed experimentally and via a FES.

Table 2.2 Geometries of the analyzed samples of the magnetic hybrid material

Geometry	Length (mm)	Width (mm)	Thickness (mm)
I	17.94	2.81	0.3
II	18.00	1.06	0.02

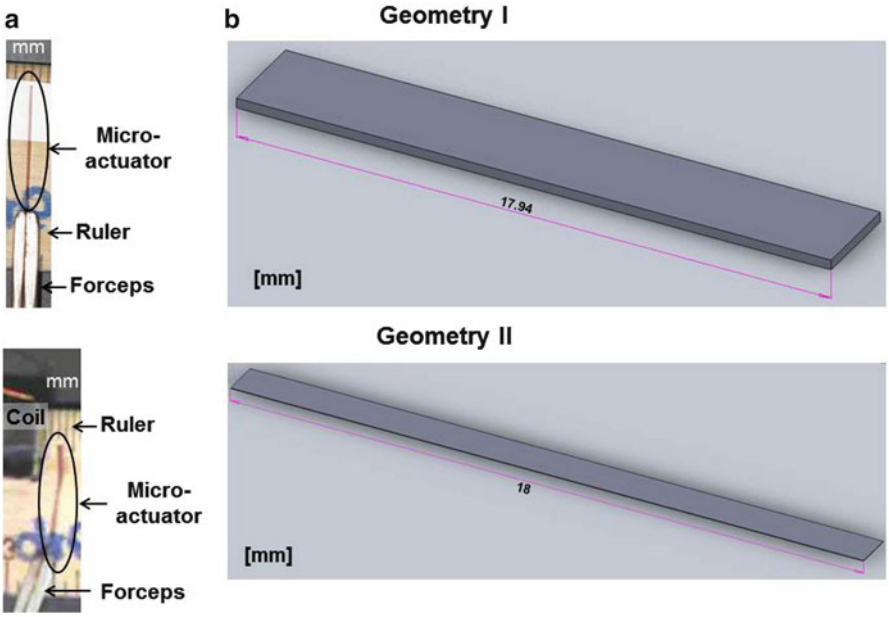

Fig. 2.14 Geometries of the magnetic hybrid actuator samples (see Table 2.2): (**a**) lateral view photograph and (**b**) schematic representation

The range of variation of the magnetic field for both analyses, experimental and FES, is based on previous results, which indicates a magnetic field around 100 Oe necessary to excite the magnetic hybrid material. The geometries of the two samples analyzed are described and illustrated in Table 2.2 and Fig. 2.14. Both geometries seam to a long beam.

Next sections will describe the basic theory of magnetics and bending beams involved in the actuation study of the magnetic hybrid material, as well as the procedures and results concerning the experimental and simulated actuation response of the material.

2.4.1 Basic Theory

The following section shows a summary of the relevant theory in magnetics and bending of beams involved in the actuation response of the magnetic hybrid material.

Concerning magnetic equations, two vectorial variables are used to describe magnetic fields: the magnetic field strength **H**, in Ampere per meter (A/m), and the magnetic induction **B**, in Tesla (T). When an external field **H** is applied to the material, the magnetic field **B** is induced in the material. The two variables are the same only in free space; otherwise, they are connected by the equation $\mathbf{B} = \mu_0 \mathbf{H}$, where $\mu_0 = 4\pi \times 10^{-7}$ (Tm/A) is the magnetic permeability of the free space.

The magnetic force acting on a magnetic particle inside a magnetic field depends on the volume of the particle V (in m^3), the difference in the magnetic susceptibilities $\chi_p - \chi_m$ (dimensionless) between the volume susceptibility of the particle χ_p and the volume susceptibility of the medium χ_m, the magnetic permeability of free space μ_0, and the strength and gradient of the applied magnetic field **H** [19,31,34]:

$$\mathbf{F} = \mu_0 V \left(\chi_p - \chi_m\right) (\mathbf{H} \cdot \nabla) \mathbf{H} \tag{2.2}$$

For diamagnetic medium, as carboxymethyl cellulose, the volume susceptibility χ_m can be neglected and (2.2) becomes:

$$\mathbf{F} = \mu_0 V \chi_p (\mathbf{H} \cdot \nabla) \mathbf{H} \tag{2.3}$$

When the material is placed in the magnetic field, a magnetic dipole moment **m** (in Am^2) is induced in the material. The sum of the dipole moments in a volume of the material is the magnetization M, given by:

$$\mathbf{M} = \frac{\mathbf{m}}{V} \tag{2.4}$$

In a uniform magnetic field **B**, a magnetic dipole experiences a magnetic torque defined by:

$$\mathbf{T} = \mathbf{m} \times \mathbf{B} \tag{2.5}$$

This torque tends to line up the magnetic moment with the magnetic field, so this represents its lowest energy configuration.

Considering bending equations, simplifying approximations are employed to study problems of beam bending. Euler–Bernoulli beam theory is one of them [5]. It provides a means of calculating the load-carrying and deflection characteristics of beams and covers the cases for small deflections of a beam which is subjected only to lateral loads. The principal hypothesis of the Euler–Bernoulli theory is that plane sections remain plane and normal to the axis of the beam.

Considering this hypothesis, the displacement δ (in m) at the free end of a cantilever beam (rectangular cross-section) with a single concentrated load F (in N) at the same free end, is done by the expression:

$$\delta = \frac{FL^3}{3EI} \tag{2.6}$$

where E is the Young's modulus of the cantilever's material (in Pa) and $I = bh3/12$ is its area moment of inertia (in m4). The geometry of the cantilever is defined by its length L, width b, and thickness h (all in meters, m).

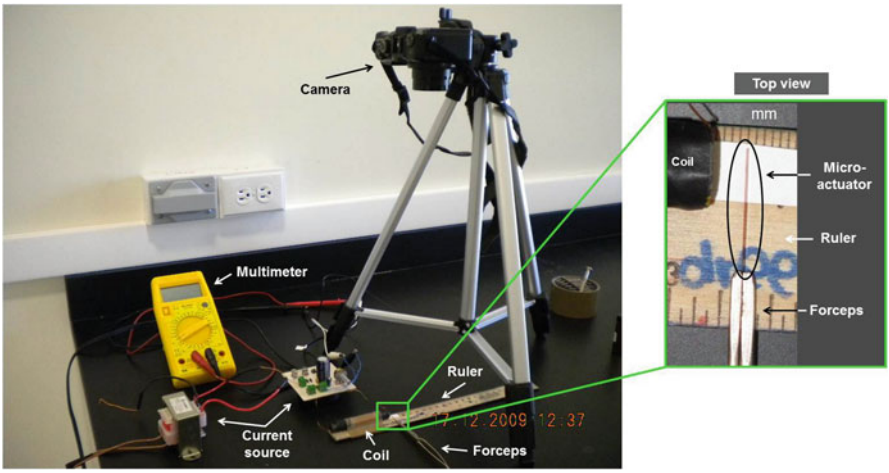

Fig. 2.15 Experimental setup to quantify the bending of the magnetic hybrid material samples

2.4.2 Experimental Actuation Response

The next study will focus on experimental evaluation of the magnetic hybrid material in an effort to determine the feasibility of utilizing these materials as bending-type actuators. This study has been realized for the two samples of the magnetic hybrid material whose geometries are described in Table 2.2. The experimental setup is shown in Fig. 2.15. After mounting the magnetic samples in a fixed-free cantilever configuration, uniform magnetic fields are applied to the samples; it causes the samples to bend, similar to a cantilever beam. The samples were oriented such that the length of the sample was perpendicular to the direction of the magnetic field. A wood ruler is placed below the sample to quantify the displacement of the bending. A digital camera Canon Powershot G10 records the experiments. In order to produce a varying magnetic field, an electrical current was supplied to a coil. The objective of this experimentation is to measure the displacement response of the magnetic hybrid material due to an external applied magnetic field. Linearity is an important characteristic for both the use and the characterization of actuators [21].

The coil has been designed using (2.7), considering a magnetic field $H = 7957.75$ A/m (100 Oe), and an electrical current $i = 1$ A. The resulting coil consists of 398 turns of 15-AWG wire wounded around a ferrite core with 5 cm of length l and 1 cm of diameter ϕ. For the two samples studied, the relationship between the applied electrical current and the resulting magnetic field using (2.7) is shown in Table 2.3.

$$N = \frac{Hl}{i} \tag{2.7}$$

Table 2.3 Relationship between electrical current and magnetic field

Sample	Current i (A)	Magnetic field H (A/m)	Magnetic field H (Oe)
I	0	0	0
	0.20	1586.69	19.94
	0.44	3441.37	43.25
	0.65	5197.88	65.32
	0.84	6689.05	84.06
	1.05	8373.92	105.23
	1.23	9809.37	123.27
	1.40	11114.81	139.67
II	0	0	0
	0.19	1544.24	19.41
	0.43	3422.80	43.01
	0.61	4855.60	61.02
	0.83	6582.92	82.72
	1.06	8461.48	106.33
	1.21	9639.56	121.13
	1.38	10984.80	138.04

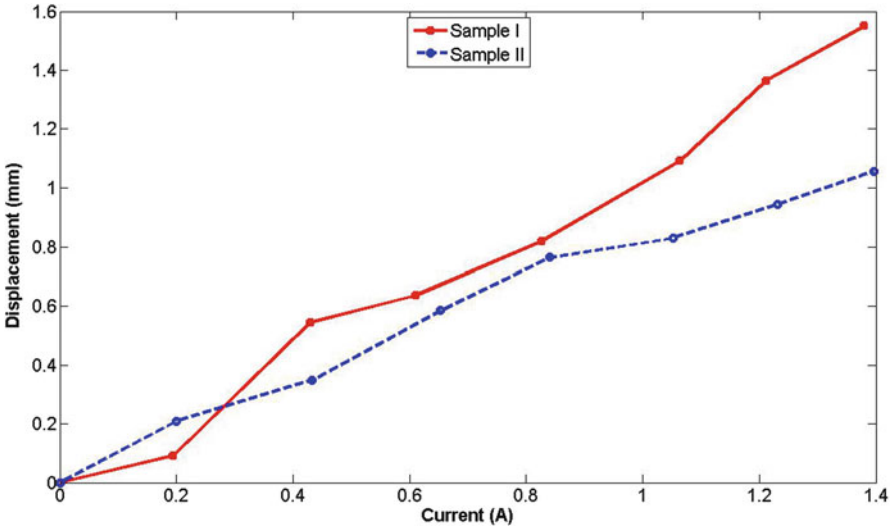

Fig. 2.16 Experimental displacement of the two samples of the magnetic hybrid material as a function of the electrical current applied to the coil

Figure 2.16 gives evidence that the geometry and shape affect the displacement response. The thinner sample, sample II, presents 48% more displacement than the bigger sample (sample I), being the maximal displacement attempted 1.55 mm. Considering an uniform distribution of the nanoparticles in the polymeric matrix, the rotation motion of the samples depends principally on the medium in which they are

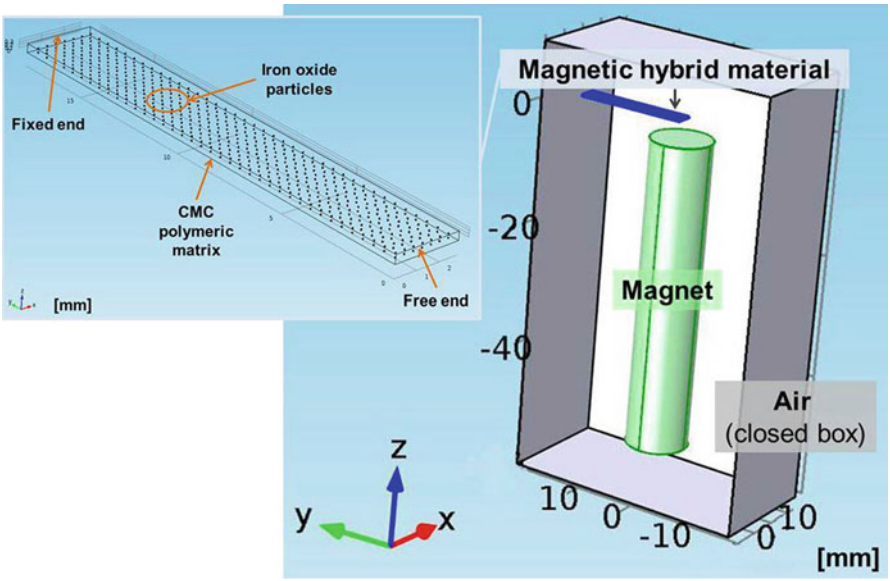

Fig. 2.17 Finite element setup of the magnetic hybrid material (sample II)

embedded. For both cases, the displacement generated by the magnetic field could show a positive linear correlation over the range studied. Hence, the magnetic hybrid material can be considered as a candidate of a flexible actuator.

Next section shows the FES results of the magnetic hybrid material.

2.4.3 Finite Element Simulation of Actuation Dynamics

As improved materials emerging, it becomes necessary to address key issues such as the need of effective magnetomechanical modeling and guiding parameters in scaling the actuators [24]. The dynamic FES of the magnetic hybrid film allows the examination of its behavior in order to extend experimental study and to validate the performance of the hybrid material.

Generally, FES on magnetic hybrid materials is done considering the material as one material [4]. The objective of this section is to present the first simulations of the magnetic hybrid material considering the two components that form it: Na-CMC and Fe_2O_3. These FES of the magnetic hybrid material as a bending-type actuator was done using COMSOL Multiphysics 4.3. We simulate the geometry of the two samples defined in Table 2.2 introducing only a limited number of particles to take into account the magnetic effect produced by the iron oxide particles and the viscoelastic effect inherent to the carboxymethyl cellulose.

Figure 2.17 shows the simulated setup of the samples. The varying magnetic field has been simulated as a permanent magnet with a magnetization varying linearly

Table 2.4 Physical parameters of the simulated samples

Parameter	Young's module (MPa)	Poisson's ratio	Density (kg/m^3)	Relative permeability $(1+\chi)$
Values for CMC [1,4,9,23]	6.37	0.35	1.59	1
Values for Fe_2O_3 [2,6,13,34]	18.82	0.3	1,089	7

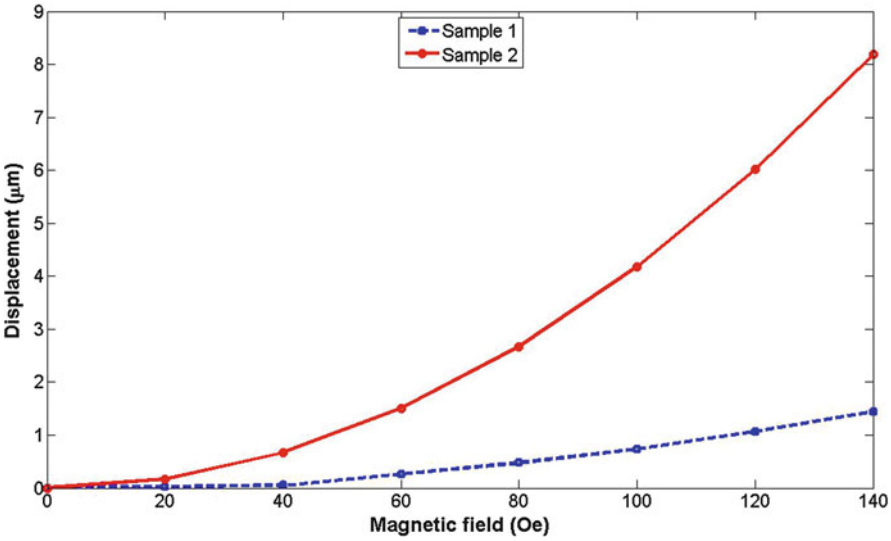

Fig. 2.18 FES displacement of the magnetic hybrid material face to an external magnetic field

from 0 to 140 Oe. The iron oxide (Fe_2O_3) particles, as spheres, are embedded on the polymeric matrix beam. The sample I contains 528 particles whose diameter is 0.1 mm, and the sample II contains 348 particles of 0.015 mm of diameter. Table 2.4 describes the physical parameters for the CMC and the Fe_2O_3 considered for the FES.

The simulation has been developed in two steps. First, we evaluate the magnetic forces acting on the superparamagnetic particles due to the permanent magnet. Second, we simulate the displacement of the hybrid material produced by these magnetic forces. Meshed models consist of triangular elements on the surface and tetrahedral elements in the volume. The automatic meshing available in COMSOL Multiphysics has been used to define the meshing. Depending on the geometry of the sample, during the magnetic simulation, the mesh includes 128,268–447,198 elements which represent between 7,479 and 10,111 nodes. Considering the same conditions, during the second step of the simulation, the mesh includes 134,074–149,293 elements which represent between 7,068 and 10,178 nodes, depending on the geometry of the sample. All the simulations are done in statics conditions. The resulting curves of the displacement as a function of the magnetic field are shown in Fig. 2.18. The nonlinearity of the displacement response is a consequence of the polymeric medium in which the particles are embedded.

Results obtained by FES (Fig. 2.18) could be considered as a first approximation of experimental results (Fig. 2.16). In experimental results, the displacement seems proportional to the electrical current that produces a magnetic field; while in FES results the displacement is exponentially proportional to the simulated magnetic field. These deviations between experimental results and FES results are associated with the limited number of Fe_2O_3 nanoparticles introduced in the FES models to take into account the magnetic effect produced by the iron oxide particles into the viscoelastic effect, inherent to the carboxymethyl cellulose.

The synthesis in situ of iron oxide nanoparticles into the precursor hybrid material to obtain the magnetic hybrid material allows us to driving the viscoelasticity of CMC, because the displacements or deformations in the magnetic hybrid material can be modified as a function of the magnetic field applied.

2.5 Conclusion

On the one hand, a magnetic hybrid material consisting of nanoparticles of iron oxide in a Na-CMC matrix was obtained. The synthesis of magnetic nanoparticles from the precursor hybrid material was confirmed via XRD and IR analysis. The iron oxide nanoparticles are embedded in the Na-CMC and their measured size was around 4 nm, having a nearly spherical morphology. The analysis of the magnetic properties of the magnetic hybrid material shows a superparamagnetic behavior at room temperature changing to ferromagnetic below 71 K, the blocking temperature. Our results suggest that in situ precipitation of nanoparticles in the precursor hybrid material is a promising route to the production of the magnetic hybrid material.

On the other hand, the dynamic response, specifically the displacement of the magnetic hybrid material, has been observed in order to probe the feasibility to use this material as a bending-type actuator. The experimental results show that the responses of the deflection have a linear trend over a reasonable range, suggesting that the magnetic hybrid material can be used as bending-type actuators in small mechanical systems and devices. The thinner sample showed the largest response among the two samples considered in this study. When an electrical current of 1.40 A is applied to the coil, the tip deflected nearly 1.55 mm. This result suggests that the dynamic experimental behavior provide promising implications for their role as magnetically controlled actuator. First simulations have been also done considering the two components of the magnetic hybrid material: the oxide iron nanoparticles and the carboxymethyl cellulose. The displacement response takes into account the viscoelastic effect of the polymeric matrix and the magnetization of the magnetic particles. Further studies must be addressed in this sense in order to describe the macroscopic magnetic behavior of the hybrid material visualizing a further application of the material working as a magnetic microactuator.

References

1. Aqualon sodium carboxymethylcellulose: physical and chemical properties. Technical Report, Hercules Incorporated, 1999
2. A.B.M. Aowlad Hossain, M.H. Cho, S.Y. Lee, Magnetic nanoparticle density mapping from the magnetically induced displacement data: a simulation study. BioMed. Eng. OnLine, 11, p. 13 (2012). doi:10.1186/1475-925X-11-11
3. M.F. Ashby, Y.J.M. Bréchet, Designing hybrid materials. Acta Mater. **51**, 5801–5821 (2003)
4. M. Barham, D. White, Finite element simulation of permanent magnetoelastic thin films. IEEE Trans. Magn. **47**(5), 1402–1405 (2011)
5. A.P. Boresi, P.C. Ken, *Elasticity in Engineering Mechanics* (PTR Prentice Hall, Englewood Cliffs, 1987)
6. J. Chatterjee, Y. Haik, C.-J. Chen, Size dependent magnetic properties of iron oxide nanoparticles. J. Magn. Magn. Mater. **257**(1), 113–118 (2003)
7. O. Cugat, J. Delamare, R. Gilbert, Magnetic microsystems: Mag-MEMS, in *Magnetic Nanostructures in Modern Technology* (Springer, Berlin, 2008), pp. 105–125
8. D. Eder, Carbon nanotube-inorganic hybrids. Chem. Rev. **110**(3), 1348–1385 (2010)
9. T.J. Fiske, H. Gokturk, D.M. Kalyon, Enhancement of the relative magnetic permeability of polymeric composites with hybrid particulate fillers. J. Appl. Polym. Sci. **65**(7), 1371–1377 (1997)
10. M.A. Garza-Navarro, M. Hinojosa-Rivera, V.A. González-González, Desarrollo de nanocompuestos superparamagnticos quitosán/magnetita. Ingenierías **9**(33), 14–20 (2006)
11. M.A. Garza-Navarro, M.E. Reyes-Melo, V. González-González, C. Guerrero-Salazar, U. Ortiz-Mendez, Modeling of isochronal complex magnetic susceptibility of polymer-magnetic nanocomposites using fractional calculus. J. Appl. Polym. Sci. **23**(4), 2154–2161 (2012)
12. S.P. Gubin, Y.A. Koksharov, G.B. Khomutov, G.Y. Yurkov, Magnetic nanoparticles: preparation, structure and properties. Russ. Chem. Rev. **74**(6), 489–520 (2005)
13. Z. Guo, K. Lei, L. Li, H.W. Ng, S. Prikhodko, H.T. Hahn, Fabrication and characterization of iron oxide nanoparticles reinforced vinyl-ester resin nanocomposites. Compos. Sci. Technol. **68**(6), 1513–1520 (2008)
14. V. Hegedusic, Z. Herceg, S. Rimac, Rheological properties of carboxymethylcellulose and whey model solutions before and after freezing. Food Technol. Biotechnol. **38**(1), 19–26 (2000)
15. C.W. Hoogendam, A. de Keizer, S.M.A. Cohen, B.H. Bijsterbosch, Adsorption mechanisms of carboxymethyl cellulose on mineral surfaces. Langmuir **14**(14), 3825–3839 (1998)
16. J.P. Jose, K. Joseph, Advances in polymer composites: macro- and microcomposites. State of the art, new challenges, and opportunities, in *Polymer Composites. Volume 1: Macro- and Microcomposites* (Wiley-VCH, Weinheim, 2012) [Chapter 1]
17. M. Karg, Multifunctional inorganic/organic hybrid microgels. An overview of recent developments in synthesis, characterization, and application. Colloid Polym. Sci. **290**(8), 673–688 (2012)
18. G. Kickelbick, *Hybrid Materials: Synthesis, Characterization and Applications* (Wiley-VCH, Weinheim, 2007)
19. M.-C. Kim, D.-K. Kim, S.-H. Lee, M.S. Amin, I.-H. Park, C.-J. Kim, M. Zahn, Dynamic characteristics of superparamagnetic iron oxide nanoparticles in a viscous fluid under an external magnetic field. IEEE Trans. Magn. **42**(4), 979–982 (2006)
20. S.-H. Kim, S. Hashi, K. Ishiyama, Methodology of dynamic actuation for flexible magnetic actuator and biomimetic robotics application. IEEE Trans. Magn. **46**(6), 1366–1369 (2010)
21. J.-H. Koo, A. Dawson, H.-J. Jung, Characterization of actuation properties of magnetorheological elastomers with embedded hard magnetic particles. J. Intell. Mater. Syst. Struct. **23**(9), 1049–1054 (2012)
22. D. Lee, S. Kim, Y.-L. Park, R.J. Wood, Design of centimeter-scale inchworm robots with bidirectional claws, in *Proceedings of IEEE International Conference on Robotics and Automation (ICRA)*, Shanghai, China, May 2011, pp. 3197–3204

23. L.P. Li, W. Herzog, R.K. Korhonen, J.S. Jurvelin, The role of viscoelasticity of collagen fibers in articular cartilage: axial tension versus compression. Med. Eng. Phys. **27**(1), 51–57 (2005)
24. C. Liu, Y. Bar-Cohen, Scaling laws of microactuators and potential applications of electroactive polymers in MEMS, in *Proceedings of SPIE International Symposium on Smart Structures and Materials*, CA, USA, March 1999, 10 pp.
25. B. López-Walle, E. Reyes-Melo, E. López-Cuellar, Los materiales híbridos en el desarrollo de sistemas mecatrónicos. Ingenierías **14**(53), 35–43 (2011)
26. J.F. Luna-Martínez, Síntesis y caracterización de materiales nanoestructurados a base de una matriz polimérica de carboximetilcelulosa, Ph.D. thesis, Universidad Autnoma de Nuevo León, FIME, 2011
27. J.F. Luna-Martínez, E. Reyes-Melo, V. González-González, A. Torres-Castro, C. Guerrero-Salazar, S. Sepúlveda-Guzmán, Iron oxide nanoparticles obtained from a Fe(II)-chitosan polymer film. Mater. Sci. Forum **644**, 51–55 (2010)
28. J.F. Luna-Martínez, D.B. Hernández-Uresti, M.E. Reyes-Melo, C.A. Guerrero-Salazar, S. Sepúlveda-Guzmán, V.A. González-González, Synthesis and optical characterization of ZnS–sodium carboxymethyl cellulose nanocomposite films. Carbohydr. Polym. **84**, 566–570 (2011)
29. J.F. Luna-Martínez, E. Reyes-Melo, V. González-González, C. Guerrero-Salazar, A. Torres-Castro, S. Sepúlveda-Guzmán, Synthesis and characterization of a magnetic hybrid material consisting of iron oxide in a carboxymethyl cellulose matrix. J. Appl. Polym. Sci. **127**(3), 2325–2331 (2013)
30. C. Michelina, B. Flavia, Synthesis and characterization of amorphous and hybrid materials obtained by sol–gel processing for biomedical applications, in *Biomedical Science, Engineering and Technology*, Rijeka, Croatia (InTech, 2012), pp. 389–416 [Chapter 6]
31. N. Pamme, Magnetism and microfluidics. Lab Chip **6**, 24–38 (2006)
32. PRWeb, Global magnetic sensors market to reach $3.2 billion by 2017, according to a new report by Global Industry Analysts, Inc., August 2011
33. M.E. Reyes-Melo, J.F. Luna-Martínez, V.A. González-González, Materiales híbridos magnéticos. Ingenierías **14**(53), 6–12 (2011)
34. S.S. Shevkoplyas, A.C. Siegel, R.M. Westervelt, M.G. Prentiss, G.M. Whitesides, The force acting on a superparamagnetic bead due to an applied magnetic field. Lab Chip **7**, 1294–1302 (2007)
35. J. Streque, A. Talbi, R. Viard, P. Pernod, V. Preobrazhensky, Elaboration and test of high energy density magnetic micro-actuators for tactile display applications. Procedia Chem. **1**(1), 694–697 (2009)
36. W. Wang, A. Wanga, Nanocomposite of carboxymethyl cellulose and attapulgite as a novel pH-sensitive superabsorbent: synthesis, characterization and properties. Carbohydr. Polym. **82**, 83–91 (2010)
37. Y. Xiaotun, X. Lingge, N.S. Choon, C.S. Hardy, Magnetic and electrical properties of polypyrrole-coated γ-Fe_2O_3 nanocomposite particles. Nanotechnology **14**(6), 624–629 (2003)
38. Y. Yamanishi, S. Sakuma, K. Onda, F. Arai, Powerful actuation of magnetized microtools by focused magnetic field for particle sorting in a chip. Biomed. Devices **12**(4), 745–752 (2010)
39. H. Yan, M. Guo, K. Liu, Multifunctional magnetic hybrid nanoparticles as a nanomedical platform for cancer-targeted imaging and therapy, in *Biomedical Science, Engineering and Technology*, Rijeka, Croatia (InTech, 2012), pp. 283–300 [Chapter 12]

http://www.springer.com/978-1-4614-6683-3

Smart Materials-Based Actuators at the Micro/Nano-Scale
Characterization, Control, and Applications
Rakotondrabe, M. (Ed.)
2013, XII, 271 p. 145 illus., 123 illus. in color.,
Hardcover
ISBN: 978-1-4614-6683-3